Article

A New SOC Estimation for LFP Batteries: Application in a 10 Ah Cell (HW 38120 L/S) as a Hysteresis Case Study

Younghwi Ko and Woojin Choi *

Department of Electrical Engineering, Soongsil University, Seoul 06978, Korea; younghwiko93@gmail.com
* Correspondence: cwj777@ssu.ac.kr; Tel.: +82-2-820-0652

Abstract: An accurate state of charge (SOC) estimation of the lithium iron phosphate battery (LiFePO$_4$) is one of the most important functions for the battery management system (BMS) for electric vehicles (EVs) and energy storage systems (ESSs). However, an accurate estimation of the SOC of LiFePO$_4$ is challenging due to the hysteresis phenomenon occurring during the charge and discharge. Therefore, an accurate modeling of the hysteresis phenomenon is essential for reliable SOC estimation. The conventional hysteresis modeling methods, such as one-state hysteresis modeling and parallelogram modeling, are not good enough to achieve high-accuracy SOC estimation due to their errors in the approximation of the hysteresis contour. This paper proposes a novel method for accurate hysteresis modeling, which can provide a significant improvement in terms of the accuracy of the SOC estimation compared with the conventional methods. The SOC estimation is performed by using an extended Kalman filter (EKF) and the parameters of the battery are estimated by using auto regressive exogenous (ARX) model and the recursive least square (RLS) filter. The experimental results with the conventional and proposed methods are compared to show the superiority of the proposed method.

Keywords: SOC estimation; hysteresis modeling; lithium iron phosphate battery; extended Kalman filter

1. Introduction

Rechargeable lithium batteries are widely used for electric vehicles (EVs) and energy storage systems (ESSs). Lithium is a very attractive material for batteries due to its low equivalent weight and high standard potential. The first lithium ion battery was introduced to the market by Sony Corporation in 1992, and the market for these has grown to several hundreds of millions of cells per year for consumer applications. Most of them are composed of a carbon negative electrode and a lithium cobalt oxide (LiCoO$_2$) positive electrode [1]. Lithium chemistry provides higher power and energy densities in both gravimetric and volumetric terms, which makes it suitable for applications such as smart phones, digital cameras, and laptops [2]. After the lithium iron phosphate (LiFePO$_4$) battery was introduced by replacing the expensive cathode material with LiCoO$_2$, the cost of the battery was reduced by 10% to 50% [3]. Compared with the other phosphate-based cathode materials, LiFePO$_4$ has lower operating voltage (2.0–3.65 V) but higher capacity [4]. The use of LiFePO$_4$ offers a longer cycle life and a higher current rating over standard lithium ion batteries. Due to their advantages over other kinds of batteries, LiFePO$_4$ batteries have shown a significant growth in use of EVs and ESSs. If the LiFePO$_4$ battery is overcharged or over discharged, the battery may receive fatal damage. So, it is necessary to manage this battery so that it can be used within a safe range [5–7]. A battery management system (BMS) that can accurately estimate the state of charge (SOC) of the battery is also needed [8–10].

However, a flat Open Circuit Voltage (OCV) plateau in the range of 20% to 80% SOC makes it difficult to achieve an accurate SOC estimation [11]. LiFePO₄ batteries produce a hysteresis phenomenon and cell OCV during charge that are different from during discharge at the same SOC [12]. The hysteresis phenomenon needs to be considered carefully for an accurate SOC estimation; otherwise, the error in SOC estimation becomes quite large.

In this paper, an SOC estimation with an advanced hysteresis modeling method is proposed to achieve SOC estimation of LiFePO₄ batteries with high accuracy. In the proposed method, the conventional parallelogram method [13] is further improved by using piecewise linearization of the hysteresis contour to reduce approximation error in the conventional method. The SOC estimation is performed by using an extended Kalman filter (EKF) and the parameters of the equivalent circuit of LiFePO₄ are estimated by the auto regressive exogenous (ARX) model and the recursive least square (RLS) filter [14–16]. In order to prove the effectiveness of the proposed method, accuracy in estimating SOC by each method are compared.

2. Conventional and Proposed Hysteresis Modeling Methods for LiFePO₄ Battery

In this section, the conventional and proposed hysteresis modeling methods are presented and their advantages and disadvantages show the superiority of the proposed method.

2.1. One-State Hysteresis Modeling Method

One conventional hysteresis modeling method for the battery is one-state hysteresis model (OSHM) [17] and is applied to a LiFePO₄ battery in Reference [11,18]. An averaged OCV $(OCV_{avg}(SOC))$ as a function of SOC is described by means of OCV charge and OCV discharge extracted from the SOC–OCV curve. The function $H(SOC)$ is the difference between the averaged OCV and the OCV charge or OCV discharge, $H(SOC) = OCV_{chr} - OCV_{avg}$ or $H(SOC) = OCV_{avg} - OCV_{dis}$, as shown in Figure 1. Hence, it is positive during the charge and negative during the discharge.
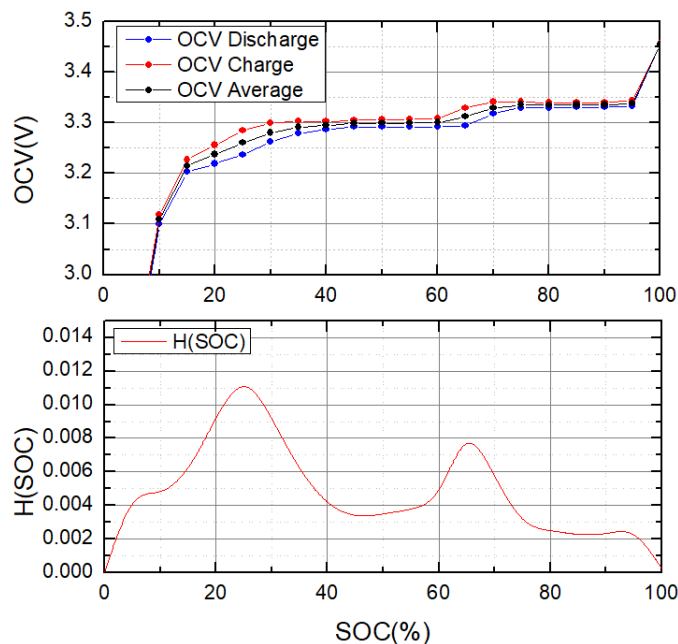

Figure 1. State of charge (SOC–OCV) curve of LiFePO4 and H(SOC) curve for one-state hysteresis modeling (OSHM).

Therefore, the actual OCV of the battery including the hysteresis can be represented as $OCV = OCV_{avg} + V_h$, where V_h is the hysteresis voltage introduced by Equation (1)

$$\frac{dV_h(SOC,t)}{dSOC} = K \cdot [H(SOC) - V_h(SOC,t)] \tag{1}$$

where K is the constant that determines the rate of voltage change where the hysteresis voltage reaches $H(SOC)$. Since $\frac{d(SOC)}{dt} = \frac{\eta_b \cdot I_b}{C_n}$ by coulomb counting, Equation (1) can be rewritten as Equation (2)

$$\frac{dV_h(SOC,t)}{dt} = K \cdot \left| \frac{\eta_b \cdot I_b}{C_n} \right| [H(SOC) - V_h(SOC,t)] \tag{2}$$

where η_b is the coulombic efficiency, I_b is the charging current, and C_n is the capacity of the battery.

Equation (2) can be written in discrete form by Equation (3).

$$V_{h,k} = exp\left(-K \cdot \left| \frac{\eta_b \cdot I_{b,k-1}}{C_n} \right| \right) \cdot V_{h,k-1} + \left(1 - exp\left(-K \cdot \left| \frac{\eta_b \cdot I_{b,k-1}}{C_n} \right| \right)\right) \cdot H(SOC_k) \tag{3}$$

The final form of the state space equation can be obtained by including the hysteresis voltage in Equation (3) and EKF is used for the SOC estimation. Though this method is simple to implement, it shows a large error in estimating SOC of the LiFePO$_4$ for which the SOC–OCV curve has a flat plateau.

2.2. Hysteresis Modeling Method by Using a Parallelogram

Another conventional hysteresis modeling method is the parallelogram modeling method proposed in Reference [19]. In this method, the trajectory of the hysteresis voltage during charge/discharge is modeled by using a parallelogram and is calculated by using the charge throughput as shown in Equation (4).

$$OCV(z, \alpha) = (1 - \alpha)OCV_{dis}(z) + \alpha OCV_{chr}(z) \tag{4}$$

where α is the hysteresis factor.

The empirical equation of the hysteresis factor corresponding to the charge throughput can be expressed as follows [20]

$$\alpha = v\alpha_1 + (1 - v)\alpha_2 \tag{5}$$

$$\text{For the charge,} \begin{cases} \alpha_1 = \int h_1 \frac{I}{C_n} dt & 0 \le \alpha_1 \le 1 \\ \alpha_2 = \int h_2 \frac{I}{C_n} dt & 0 \le \alpha_2 \le 1 \end{cases} \tag{6}$$

$$\text{For the discharge,} \begin{cases} \alpha_1 = \int h_1 \frac{I}{C_n} dt & 0 \le \alpha_1 \le 1 \\ \alpha_2 = \int h_2 \frac{I}{C_n} dt & 0 \le \alpha_2 \le 1 \end{cases} \tag{7}$$

where v is the ratio of α_1 and α_2; h_1 and h_2 are the slopes of the parallelogram model. All the parameters in the hysteresis model, v, h_1, and h_1, can be extracted by using a parallelogram and the least square estimation. It is possible to calculate the hysteresis voltage accurately by the parallelogram modeling method; hence, the SOC estimation can be achieved with high accuracy. However, the error in between the actual hysteresis voltage trajectory and the parallelogram increases since both inner and outer parallelograms cannot exactly follow the hysteresis voltage as shown in Figure 2.
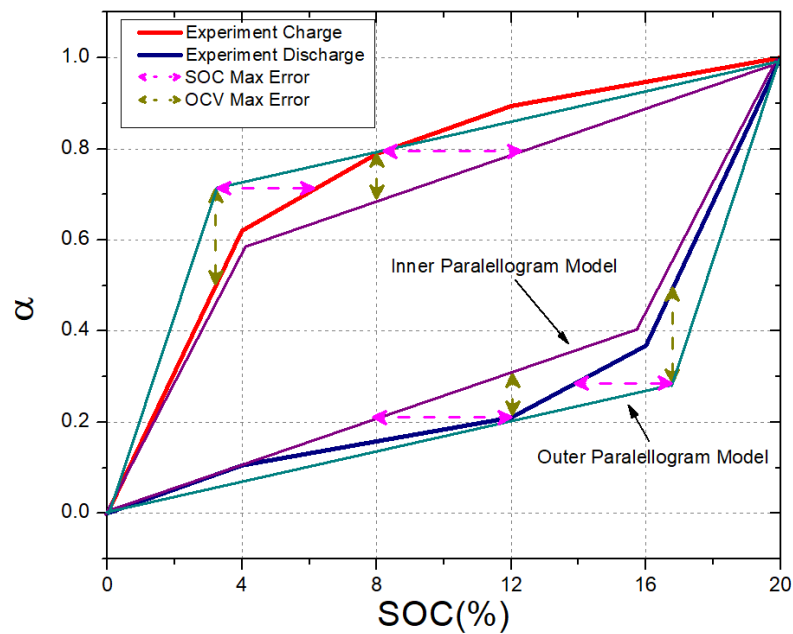
Figure 2. Parallelogram method for hysteresis modeling.

2.3. The Proposed Advanced Hysteresis Model for the LiFePO₄ Battery

　　In this section, the proposed hysteresis modeling method is described and its advantage is presented in detail. The main purpose of the hysteresis modeling is to determine whether the actual OCV at each SOC lies on the charge curve, on the discharge curve, or somewhere between them depending on the charge throughput [13]. According to the results achieved from the previous test, as depicted in Figures 3 and 4, the boundary curve is called by the major loop. The partial test with 4% ΔSOC will show a small loop lying between two boundary curves, called a minor loop. As shown in Figure 3, the charge curve and the discharge curve of the minor loop touches the major loop when the SOC varies by 20%.
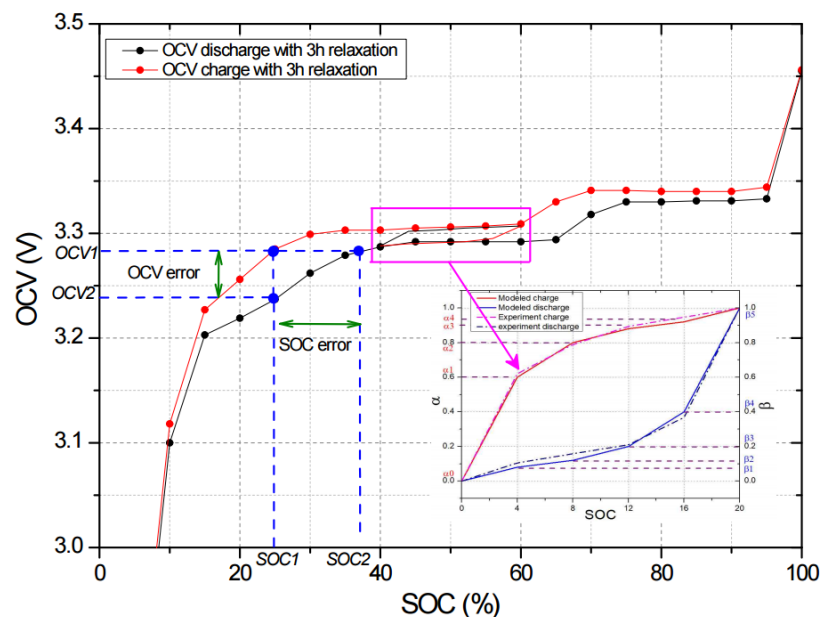

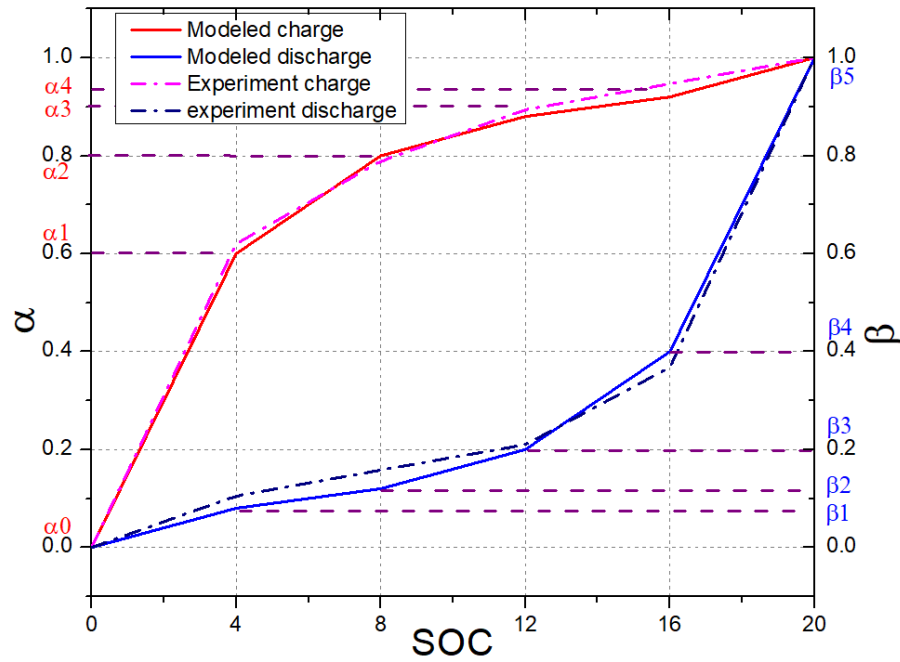**Figure 3.** SOC-OCV curve (major loop hysteresis) of LiFePO₄.

Figure 4. Proposed modeling method for the minor loop hysteresis.

The proposed method was developed to reconstruct the OCV transition caused by hysteresis. This method introduces α and β as two hysteresis factors and Δ as a change in SOC. Figure 4 shows how the method works with α, β, and Δ. Δ increases from 0 to Δn when the battery is charged, while Δ decreases from Δn to 0 when the battery is discharged. In order to model the hysteresis accurately, the variation in OCV between the upper boundary curve and the lower boundary curve are divided into five sectors as shown in Figure 4. α and β represent the ratio of hysteresis voltage change during the charge and discharge at each sector. Though Δ can be selected less than 4% to improve the accuracy, it incurs more computational burdens. Therefore, n is selected as 5 so that each step change results in 4% SOC variation. α represents the slope of the voltage change during the charge and its value varies from α_0 to α_n. β represents the slope of the voltage change during the discharge and its value varies from β_n to β_0.

Hence, the OCV during the hysteresis can be calculated according to the charge throughput as shown in the following equations.

$$OCV(SOC, \alpha) = \alpha \cdot OCV_{chr} + (1 - \alpha) \cdot OCV_{dis} \tag{8}$$

$$OCV(SOC, \beta) = \beta \cdot OCV_{chr} + (1 - \beta) \cdot OCV_{dis} \tag{9}$$

where the values of α and β are normalized between 0 to 1. The hysteresis factors are refreshed at each sector. However, when the accumulated charge throughput during the charge or discharge exceeds 20% SOC, the OCV touches the major hysteresis loop. Equations (10) and (11) show how to calculate α and β.

$$\alpha_k = \alpha_0 - \int_0^k \frac{\eta_b \cdot (\alpha_n - \alpha_{n-1}) \cdot I_{b,k,chr}}{(\Delta_n - \Delta_{n-1}) \cdot C_n} dt \tag{10}$$

$$\beta_k = \beta_0 - \int_0^k \frac{\eta_b \cdot (\beta_n - \beta_{n-1}) \cdot I_{b,k,dis}}{(\Delta_n - \Delta_{n-1}) \cdot C_n} dt \tag{11}$$

Equations (10) and (11) can be represented in discrete forms as Equations (12) and (13).

$$\alpha_k = \alpha_{k-1} - \frac{\eta_b \cdot (\alpha_n - \alpha_{n-1}) \cdot I_{b,k,chr} \cdot \Delta T}{(\Delta_n - \Delta_{n-1}) \cdot C_n} \tag{12}$$

$$\beta_k = \beta_{k-1} - \frac{\eta_b \cdot (\beta_n - \beta_{n-1}) \cdot I_{b,k,dis} \cdot \Delta T}{(\Delta_n - \Delta_{n-1}) \cdot C_n} \tag{13}$$

where C_n is the available capacity, η_b is the coulomb efficiency of the battery, $I_{b,k,chr}$ is the charge current, and $I_{b,k,dis}$ is the discharge current.

3. SOC Estimation of LiFePO₄ Battery with EKF and Parameter Estimation Using ARX Model and RLS Filter

In this section the SOC estimation of LiFePO₄ battery with EKF and parameter estimation using ARX model and RLS filter is detailed.

3.1. ARX Model and RLS Filter

In order to achieve a good accuracy in SOC estimation of the battery, an accurate model of the battery needs to be used. The battery model should be capable of describing the dynamic behaviors of the battery with high accuracy and it should be simple enough to establish state equations [21]. The equivalent circuit model (ECM), consisting of resistor and parallel R-C networks connected in series, is the most commonly selected model. It was identified that two R-C networks are good enough to represent the dynamic behaviors of LiFePO₄ batteries including the relaxation voltage [22]. However, since the two R-C networks model is too complicated and the computational burden is quite high, the R-R||C model is preferred, as shown in Figure 5. Here, the voltage variation by the second R-C network is merged into the OCV by reconstructing it with the equilibrium voltage [23]. The ECM model used for the modeling is represented in Figure 5, in which Rᵢ is the pure Ohmic resistance, Rₚ is the charge transfer resistance, and the double layer capacitance is Cₚ [24].
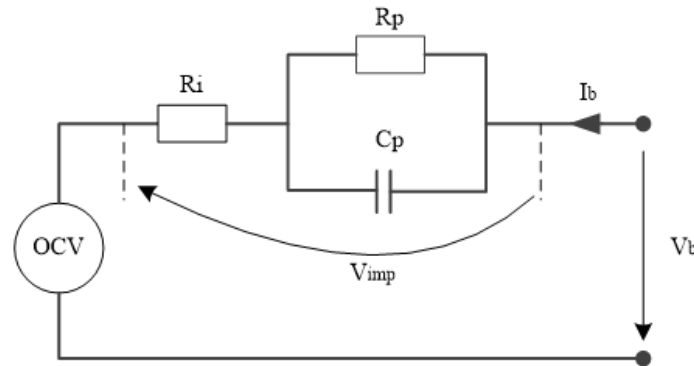

Figure 5. Equivalent circuit model of LiFePO₄ battery.

In order to estimate the SOC of the battery, the combination of the RLS and EKF is used and the parameters of the battery are obtained by the auto regressive exogenous (ARX) model in this research. The transfer function G(s) of the battery impedance can be expressed in s-domain as follows.

$$G(s) = \frac{V_b(s) - OCV(s)}{I_b(s)} = \frac{V_{imp}(s)}{I_b(s)} = R_i + \frac{R_p}{1 + s \cdot R_p \cdot C_p} \tag{14}$$

In order to convert this transfer function in a discrete form, Euler's forward transformation method is used and the resulting equation can be obtained as follows.

$$G(z^{-1}) = \frac{a_1 + a_2 \cdot z^{-1}}{1 + a_3 \cdot z^{-1}} \tag{15}$$

The impedance voltage in discrete form is shown in Equation (16).

$$V_{imp,k} = a_1 \cdot I_{b,k} + a_2 \cdot I_{b,k-1} + a_3 \cdot V_{imp,k-1} \tag{16}$$

where $a_1 = R_i$, $a_2 = \frac{T}{C_p}\left(1 + \frac{R_i}{R_p}\right)$, $a_3 = \frac{T}{R_p.C_p} - 1$, and $V_{imp,k} = OCV_k - V_{b,k}$

To identify these parameters, Equation (17) should be written in a form as

$$V_{imp,k} = \theta_k.\psi_k = [a_{1,k}, a_{2,k}, a_{3,k}][I_{b,k}; I_{b,k-1}; V_{imp,k-1}] \tag{17}$$

where ψ_k is the input vector obtained from the measured input values including the voltage drop across the battery impedance at the previous time index $V_{imp,k-1}$ and the measured battery current at current and previous time index $I_{b,k}$ and $I_{b,k-1}$.

As mentioned earlier, the RLS filter is used to identify the parameters of the battery model. The RLS filter has been widely used for online parameter identification due to its lower computational burden during the last three decades [25,26]. The step-by-step implementation of this method is shown in Table 1. The dynamic system model described in Equation (17) is used and the forgetting factor λ is introduced, which gives more weight to the current data than the previous data for the time-varying vector θ_k. After the vector θ_k is obtained, the parameters of the battery can be determined by Equation (18).

Table 1. Specification of LiFePO$_4$ HW 38120 L/S battery [27].

Name	Cylindrical LiFePO₄ Battery	Model	HW 38120 L/S
Nominal Capacity	10,000 mAh	Rated Voltage	3.2 V
Energy Density	105 Wh/kg	Internal Resistance	≤ 8 mΩ
Max. charging current	3 C (30 A)	Recommended charging current	0.5 C, 5 A × 2 h
Max. continuous discharging current	3 C (30 A)–10 C (100 A)	Recommended discharging current	1 C (10 A)
Standard. charging voltage	3.65 ± 0.05 V	Max. End-off discharged voltage	2.0 V

$$R_i = a_1, R_p = \frac{a_2 - a_1.a_3}{1 + a_3}, C_p = \frac{T}{a_2 - a_1.a_3} \tag{18}$$

Equations (16)–(18) are used to extract the battery parameters after identifying $a_{1,k}, a_{2,k}$ *and* $a_{3,k}$. All the above-mentioned procedure is summarized in Figure 6 [19].
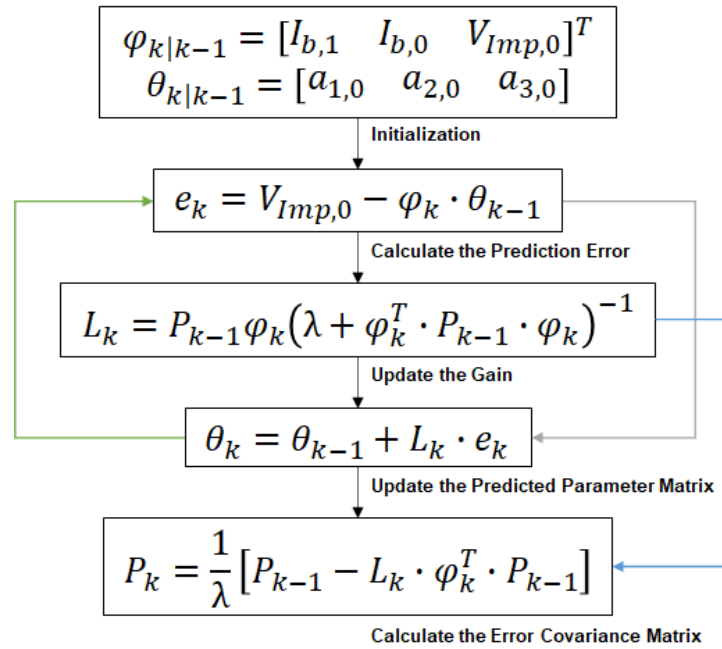
$$\varphi_{k|k-1} = [I_{b,1} \quad I_{b,0} \quad V_{Imp,0}]^T$$
$$\theta_{k|k-1} = [a_{1,0} \quad a_{2,0} \quad a_{3,0}]$$

Initialization

$$e_k = V_{Imp,0} - \varphi_k \cdot \theta_{k-1}$$

Calculate the Prediction Error

$$L_k = P_{k-1}\varphi_k \left(\lambda + \varphi_k^T \cdot P_{k-1} \cdot \varphi_k\right)^{-1}$$

Update the Gain

$$\theta_k = \theta_{k-1} + L_k \cdot e_k$$

Update the Predicted Parameter Matrix

$$P_k = \frac{1}{\lambda}\left[P_{k-1} - L_k \cdot \varphi_k^T \cdot P_{k-1}\right]$$

Calculate the Error Covariance Matrix

Figure 6. Parameter identification procedure using recursive least square filter and auto regressive exogenous (ARX) model.

3.2. Extended Kalman Filter for the SOC Estimation

The SOC of the battery can be represented through the current integration as shown in Equation (19).

$$SOC_t = SOC_0 + \int_0^t \frac{\eta_b \cdot I_b}{C_n} dt \tag{19}$$

Equation (19) can be rewritten as the discrete form as in Equation (20).

$$SOC_k = SOC_{k-1} + \frac{\eta_b \cdot I_{b,k-1} \cdot \Delta t}{C_n} \tag{20}$$

The reconstructed OCV at each time index k during the charge by Equation (8) is

$$OCV(SOC_k, h_k) = h_k \cdot OCV_{chr}(SOC_k) + (1 - h_k) \cdot OCV_{dis}(SOC_k) \tag{21}$$

where SOC_k and SOC_{k-1} are the SOC at time index k and $k-1$, respectively; $I_{b,k-1}$ is the battery current at previous time index; and Δt is the sampling period.

The EKF is a method to estimate the system state in real-time and the algorithm compares the measured terminal voltage with the estimated voltage predicted by the EKF using a battery model [28]. The difference between the predicted and the measured terminal voltage leads to an adaption of the state of the battery model to that of the real battery. Therefore, the accurate model of the battery is critical for the accurate estimation of the terminal voltage, hence the SOC estimation. The discrete-time state equations for a non-linear system can be given as

$$x_k = f(x_{k-1}, u_k) + w_k$$
$$y_k = h(x_k, u_k) + v_k \tag{22}$$

where x_k represents the state parameter, f and h are non-linear system functions, u_k is the input, w_k is the process noise vector, v_k is measurement noise vector, and y_k is the measured signal.

In order to apply the EKF to the equivalent circuit model of LiFePO₄ battery in Figure 5 , the state space equation in the discrete form can be derived as

$$x_k = \begin{bmatrix} SOC_k \\ V_{Cp,k} \end{bmatrix} = \begin{bmatrix} 1 & 0 \\ 0 & 1 - \dfrac{\Delta t}{C_p R_p} \end{bmatrix} \cdot \begin{bmatrix} SOC_{k-1} \\ V_{Cp,k-1} \end{bmatrix} + \begin{bmatrix} \dfrac{-\Delta t}{C_n} \\ \dfrac{-\Delta t}{C_p} \end{bmatrix} \cdot I_{b,k-1} + w_{k-1} \tag{23}$$

$$y_k = V_{b,k} = OCV(SOC_k, \alpha_k, \beta_k) - V_{Cp,k} - R_i \cdot I_{b,k} + v_{k-1} \tag{24}$$

The computation process of the EKF with the above state space equation is well-known and it can be summarized as shown in Figure 7 [28].
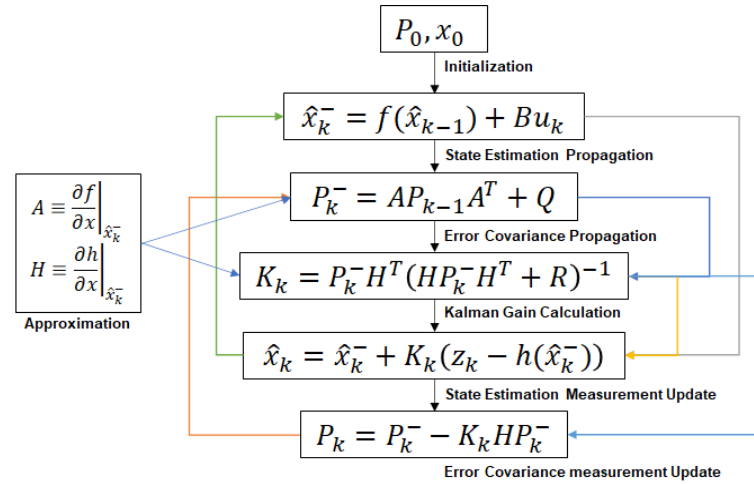

Figure 7. Computational procedure of the extended Kalman filter.

4. Experimental Results

4.1. Experiments of the SOC-OCV Curve of LiFePO₄

The tests were conducted on a LiFePO₄ HW 38120 L/S, for which specifications are shown in Table 1, by connecting it to a bipolar DC power supply (NF BP4610). A code was composed by LabVIEW 11.0 to control the output of the power supply, and voltage and current of the battery cell under test were recorded through a data acquisition board, NI PCI-6154.

In order to obtain the SOC–OCV relationship, a charge and discharge test was conducted using variable current pulses. The magnitude and duration of the current was 0.2 C and 15 min, respectively, so that each charge and discharge step charged and discharged the battery by 5% of its capacity. After each step, 3 h relaxation with no current was applied to obtain the OCV at a certain SOC. After finishing the test, two boundary OCV curves were obtained as shown in Figure 3. As shown in Figure 3, the SOC–OCV curves of the battery during the charge and discharge were not identical due to the hysteresis phenomenon. There was a gap between two curves of which the maximum value was 45 mV.

After each current pulse, the battery took 3 h relaxation and the terminal voltage was measured to obtain 3 min and 3 h relaxation voltage, OCV_{3m} and OCV_{3h}, respectively. The cell voltage recovery over several minutes or hours could not be reproduced with the simple equivalent circuit model given in Figure 5. Hence, the OCV recovery effect had to be considered separately. It was assumed that the voltage dropped across the impedance of the battery model and vanished after resting 3 min and the OCV recovery remained only. In order to incorporate the OCV recovery during the rest time, recovery factor ζ was introduced as shown in Equation (25). Here, ζ indicates whether the OCV is completely recovered or not and the transition from $\zeta = 1$ to $\zeta = 0$ during rest periods is assumed to proceed as a first-order exponential equation with the time constant of the OCV recovery

[13]. Therefore, the OCV during the hysteresis lies in between them and can be modeled as a time constant τ and the diffusion factor ζ can be calculated by using Equation (25).

$$\zeta = exp\left(\frac{180 - t}{\tau}\right) \tag{25}$$

where t is the relaxation time. If the relaxation is less than 3 min (180 s), ζ is equal to 1. Therefore, the OCV can be reconstructed using ζ as follows

$$OCV_{chr}(SOC, \zeta) = \zeta \cdot OCV_{3h,chr} + (1 - \zeta) \cdot OCV_{3m,chr} \tag{26}$$

$$OCV_{dis}(SOC, \zeta) = \zeta \cdot OCV_{3h,dis} + (1 - \zeta) \cdot OCV_{3m,dis} \tag{27}$$

where OCV_{chr} and OCV_{dis} are the OCV during the charge and discharge considering the relaxation, respectively.

4.2. Experiments for the Hysteresis Curve of LiFePO₄

In order to model the hysteresis, the hysteresis test had to be performed. Some partial cycles were applied to obtain hysteresis curves between two boundary OCV curves. At first, the fully charged battery was discharged to 20% SOC and charged up to 40% SOC by using five current pulses with 4% ΔSOC as shown in Figure 8. Next, the cell was discharged with the same current pulses. After each pulse the battery was rested for 3 h to obtain the OCV. The test was repeated at different SOCs such as 40% to 60% and 70% to 90% SOC to verify the hysteresis behavior. We found that the partial cycles at different SOCs were all the same, as shown in Figure 9. The hysteresis factors can be calculated for every 4% interval of the hysteresis curve from the experimental results.
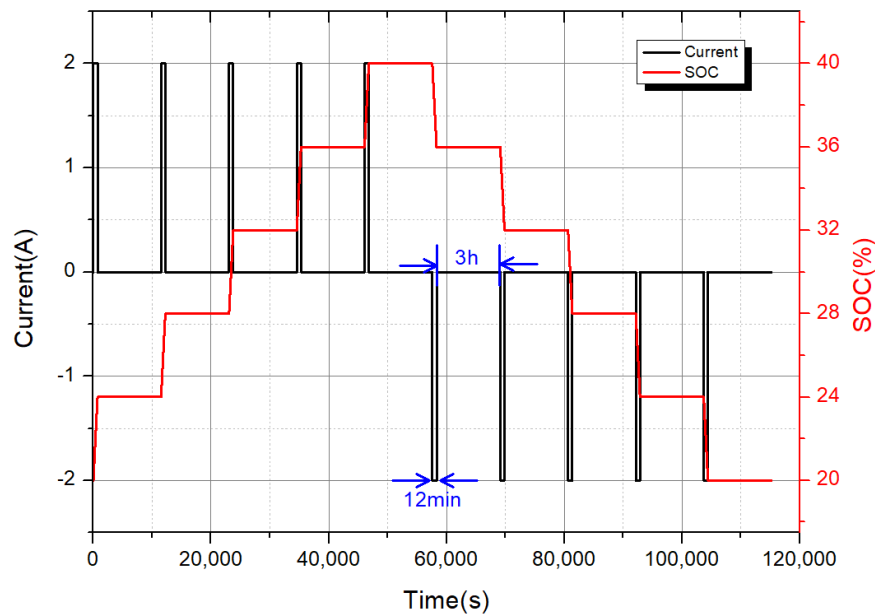

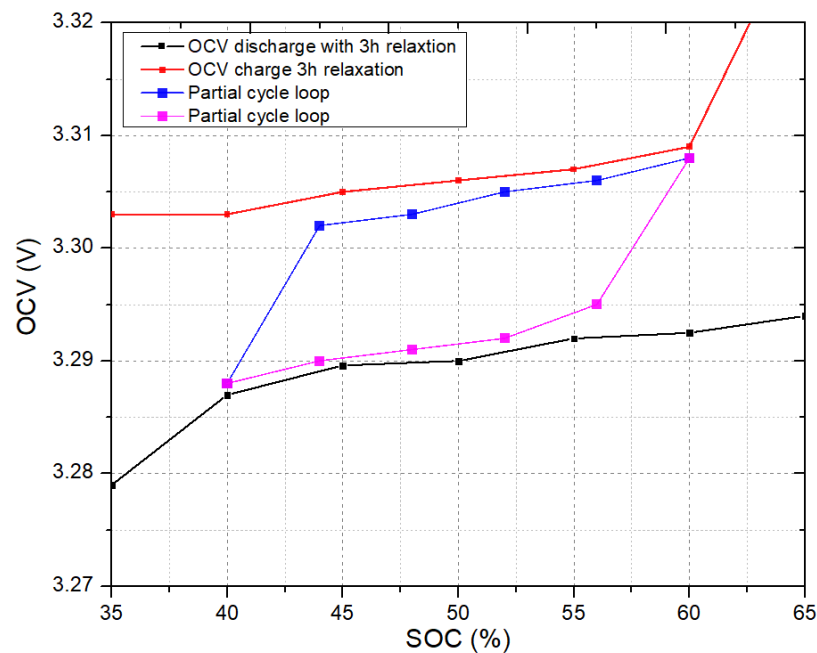**Figure 8.** Pulse currents used for the minor loop hysteresis test.

Figure 9. Experimental results of the minor loop hysteresis.

4.3. Experimental Verification

To verify the proposed hysteresis modeling algorithm at different SOC regions, the battery was fully charged to 100% SOC and discharged to 20% SOC, as shown in Figure 10. Then the battery underwent the charge and discharge process repeatedly at various SOC values. This current profile applied to the battery test is suitable to verify the accuracy of the hysteresis modeling since the hysteresis phenomenon occurs at many different SOCs.
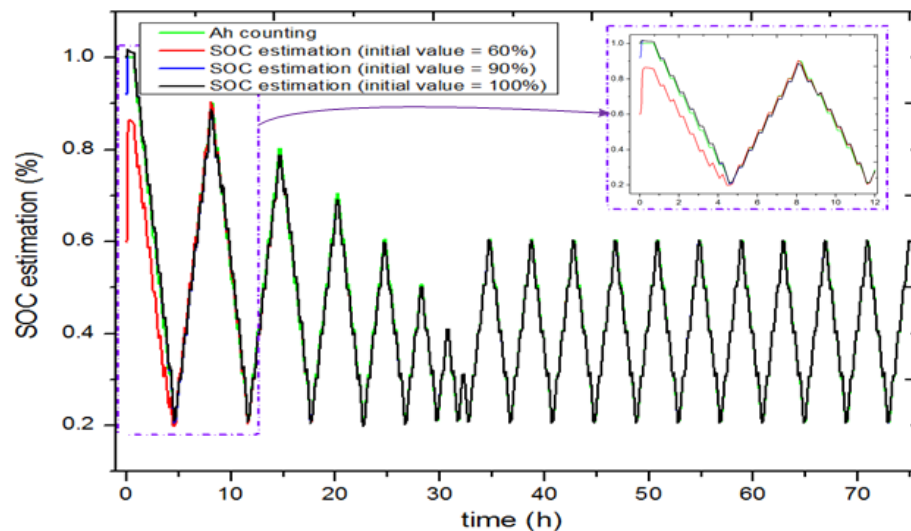

Figure 10. SOC estimation result with different initial values.

In the experiments, the Ah counting method with known initial SOC value was used as an SOC reference for the comparison. In order to confirm the performance of SOC estimation by EKF, three different initial values, 60%, 90%, and 100% SOC, were given at the beginning. Figure 10 shows the results of the SOC estimation with three different initial

SOC values and Figure 11 shows the error between the results by the proposed method and the Ah counting. Though the time for the convergence of each SOC estimation with different initial value was different: all of them converged successfully within 4 h and all the SOC estimation error after the convergence did not exceed 2%, which proves the reliable performance of the proposed method.
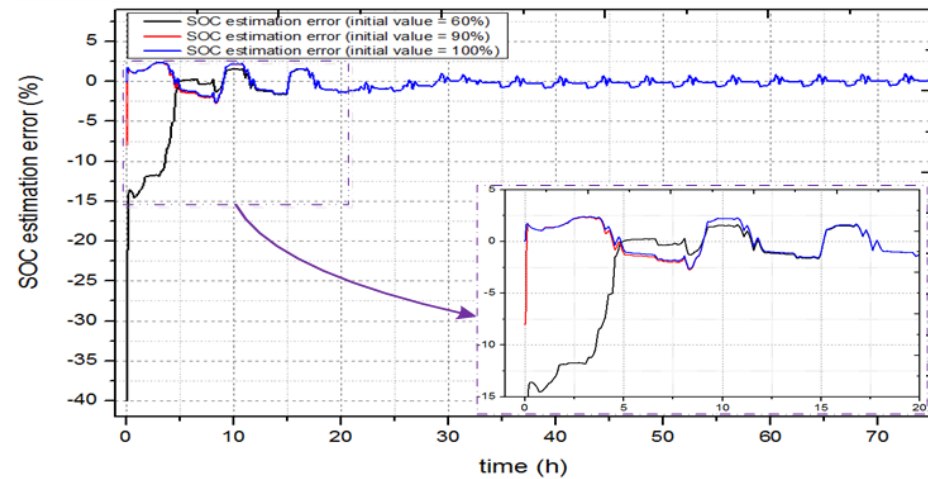

Figure 11. SOC estimation error with different initial values.

4.4. Comparison of the Methods by SOC Estimation Error

In order to compare the performance of the SOC estimation with different hysteresis modeling methods, each method was implemented separately and the results are compared in Figure 12. The root mean square error (RMSE) in Equation (28), mean absolute error (MAE) in Equation (29), and maximum error were used to evaluate the effectiveness of estimation. Here, MAE shows the size of the error intuitively and RMSE shows the distribution of the error
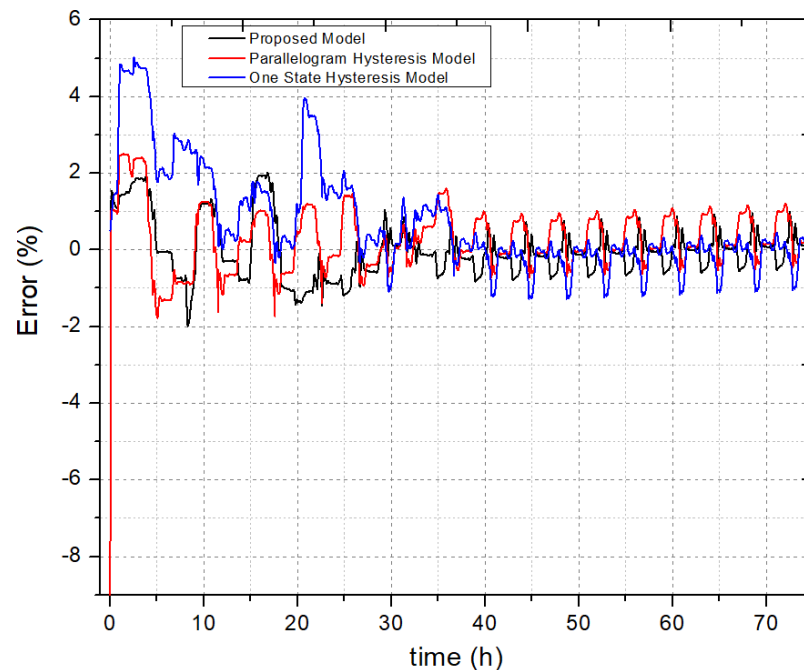

Figure 12. SOC estimation errors of three different hysteresis modeling methods.

$$RMSE = \sqrt{\frac{\sum_{k=1}^{n} e_k^2}{n}} \tag{28}$$

$$MAE = \frac{\sum_{k=1}^{n} |e_k|}{n} \tag{29}$$

where e_k is the SOC estimation error at time index k.

The SOC estimation errors with three different hysteresis models are summarized in Table 2.

Table 2. Root mean square error (RMSE), mean absolute error (MAE), and max. error of SOC Estimation with different hysteresis models.

Model	Proposed Model	Parallelogram Model	OSHM
RMSE	0.69%	0.87%	1.51%
MAE	0.47%	0.66%	0.95%
Max. Error	2.02%	2.50%	5.01%

The results in Figure 12 and Table 2 indicate that the SOC estimation by the proposed hysteresis model shows the lowest RMSE, MAE and maximum error, thereby proving the superior performance of the proposed hysteresis modeling method.

5. Conclusions

In this study, the hysteresis phenomenon of a LiFePO$_4$ battery was investigated and an advanced hysteresis modeling method was proposed. The validity of the proposed hysteresis modeling was verified through the comparison of the SOC estimation errors with the other two conventional methods. Due to the precise modeling of the hysteresis phenomenon in LiFePO$_4$ battery, the SOC estimation can be achieved with higher accuracy. The proposed hysteresis modeling can also be applied to the SOC estimation of other batteries, such as a lead-acid battery, which exhibits a significant hysteresis phenomenon.

Author Contributions: Y.K. wrote the manuscript, designed the algorithm of proposed method, analyzed the algorithm of the proposed method, and helped in preparing the final manuscript.; W.C. reviewed the manuscript and supervised the research. All authors have read and agreed to the published version of the manuscript.

Conflicts of Interest: The authors declare no conflict of interest.

Abbreviations

The following abbreviations are used in this manuscript:

SOC	state of charge
BMS	battery management system
EVs	electric vehicles
ESSs	energy storage systems
EKF	extended Kalman filter
ARX	auto regressive exogeneous
RLS	recursive least square
LiFePO$_4$	lithium iron phosphate
LiCoO2	lithium cobalt oxide
OSHM	one state hysteresis model
ECM	equivalent circuit model
RMSE	root mean square
MAE	mean absolute error

References

1. Ritchie, A. Recent developments and future prospects for lithium rechargeable batteries☆. *J. Power Sources* **2001**, *96*, 1–4, doi:10.1016/s0378-7753(00)00673-x.
2. Wang, Y.; Liu, B.; Li, Q.; Cartmell, S.; Ferrara, S.; Deng, Z.D.; Xiao, J. Lithium and lithium ion batteries for applications in microelectronic devices: A review. *J. Power Sources* **2015**, *286*, 330–345, doi:10.1016/j.jpowsour.2015.03.164.
3. Fergus, J.W. Recent developments in cathode materials for lithium ion batteries. *J. Power Sources* **2010**, *195*, 939–954, doi:10.1016/j.jpowsour.2009.08.089.
4. Satyavani, T.; Kumar, A.S.; Rao, P.S. Methods of synthesis and performance improvement of lithium iron phosphate for high rate Li-ion batteries: A review. *Eng. Sci. Technol. Int. J.* **2016**, *19*, 178–188, doi:10.1016/j.jestch.2015.06.002.
5. Aiello, O. Electromagnetic Susceptibility of Battery Management Systems' ICs for Electric Vehicles: Experimental Study. *Electronics* **2020**, *9*, 510, doi:10.3390/electronics9030510.
6. Luo, X.; Kang, L.; Lu, C.; Linghu, J.; Lin, H.; Hu, B. An Enhanced Multicell-to-Multicell Battery Equalizer Based on Bipolar-Resonant LC Converter. *Electronics* **2021**, *10*, 293, doi:10.3390/electronics10030293.
7. Aiello, O.; Crovetti, P.S.; Fiori, F. Susceptibility to EMI of a Battery Management System IC for electric vehicles. In Proceedings of the 2015 IEEE International Symposium on Electromagnetic Compatibility (EMC), Dresden, Germany, 16–22 August 2015; pp. 749–754.
8. Xing, Y.; Ma, E.W.M.; Tsui, K.L.; Pecht, M. Battery Management Systems in Electric and Hybrid Vehicles. *Energies* **2011**, *4*, 1840–1857, doi:10.3390/en4111840.
9. Lelie, M.; Braun, T.; Knips, M.; Nordmann, H.; Ringbeck, F.; Zappen, H.; Sauer, D.U. Battery Management System Hardware Concepts: An Overview. *Appl. Sci.* **2018**, *8*, 534, doi:10.3390/app8040534.
10. Doridant, A.; Abouda, K.; Givelin, P.; Thibaud, B. Battery Management System Demonstrator Board design using EMC System simulation. In Proceedings of the 2019 International Symposium on Electromagnetic Compatibility-EMC EUROPE, Barcelona, Spain, 2–6 September 2019; pp. 427–432.
11. Dong, G.; Wei, J.; Zhang, C.; Chen, Z. Online state of charge estimation and open circuit voltage hysteresis modeling of LiFePO4 battery using invariant imbedding method. *Appl. Energy* **2016**, *162*, 163–171, doi:10.1016/j.apenergy.2015.10.092.
12. Barai, A.; Widanage, W.D.; Marco, J.; McGordon, A.; Jennings, P. A study of the open circuit voltage characterization technique and hysteresis assessment of lithium-ion cells. *J. Power Sources* **2015**, *295*, 99–107, doi:10.1016/j.jpowsour.2015.06.140.
13. Roscher, M.A.; Sauer, D.U. Dynamic electric behavior and open-circuit-voltage modeling of LiFePO4-based lithium ion secondary batteries. *J. Power Sources* **2011**, *196*, 331–336, doi:10.1016/j.jpowsour.2010.06.098.
14. Windarko, N.A.; Choi, J.-H. LiPB Battery SOC Estimation Using Extended Kalman Filter Improved with Variation of Single Dominant Parameter. *J. Power Electron.* **2012**, *12*, 40–48, doi:10.6113/jpe.2012.12.1.40.
15. Xie, J.; Ma, J.; Sun, Y.; Li, Z. Estimating the State-of-Charge of Lithium-Ion Batteries Using an H-Infinity Observer with Consideration of the Hysteresis Characteristic. *J. Power Electron.* **2016**, *16*, 643–653, doi:10.6113/jpe.2016.16.2.643.
16. Pavkovic, D.; Krznar, M.; Komljenovic, A.; Hrgetic, M.; Zorc, D. Dual EKF-Based State and Parameter Estimator for a LiFePO 4 Battery Cell. *J. Power Electron.* **2017**, *17*, 398–410, doi:10.6113/JPE.2017.17.2.398.
17. Gregory L. Plett, Extended Kalman filtering for battery management systems of LiPB-based HEV battery packs: Part 3. State and parameter estimation. *J. Power Sources* **2004**, *134*, 277–292.
18. Mastali, M.; Vazquez-Arenas, J.; Fraser, R.; Fowler, M.; Afshar, S.; Stevens, M. Battery state of the charge estimation using Kalman filtering. *J. Power Sources* **2013**, *239*, 294–307, doi:10.1016/j.jpowsour.2013.03.131.
19. Duong, V.-H.; Tran, N.-T.; Park, Y.-J.; Choi, W. Novel Estimation Technique for the State-of-Charge of the Lead-Acid Battery by using EKF Considering Diffusion and Hysteresis Phenomenon. *Trans. Korean Inst. Power Electron.* **2014**, *19*, 139–148, doi:10.6113/tkpe.2014.19.2.139.
20. Mauracher, P.; Karden, E. Dynamic modelling of lead/acid batteries using impedance spectroscopy for parameter identification. *J. Power Sources* **1997**, *67*, 69–84, doi:10.1016/s0378-7753(97)02498-1.
21. Xia, B.; Chen, C.; Tian, Y.; Wang, M.; Sun, W.; Xu, Z. State of charge estimation of lithium-ion batteries based on an improved parameter identification method. *Energy* **2015**, *90*, 1426–1434, doi:10.1016/j.energy.2015.06.095.
22. He, H.; Zhang, X.; Xiong, R.; Xu, Y.; Guo, H. Online model-based estimation of state-of-charge and open-circuit voltage of lithium-ion batteries in electric vehicles. *Energy* **2012**, *39*, 310–318, doi:10.1016/j.energy.2012.01.009.
23. Duong, V.H.; Tran, N.T.; Choi, W.; Kim, D.-W. State Estimation Technique for VRLA Batteries for Automotive Applications. *J. Power Electron.* **2016**, *16*, 238–248, doi:10.6113/jpe.2016.16.1.238.
24. Waag, W.; Käbitz, S.; Sauer, D.U. Experimental investigation of the lithium-ion battery impedance characteristic at various conditions and aging states and its influence on the application. *Appl. Energy* **2013**, *102*, 885–897, doi:10.1016/j.apenergy.2012.09.030.
25. *System Identification Theory for the User, Lennart Ljung*; Linkoping University: Linköping, Sweden, 1999.
26. Jiang, J.; Zhang, Y. A revisit to block and recursive least squares for parameter estimation. *Comput. Electr. Eng.* **2004**, *30*, 403–416.
27. AA Portable Power Corp. Available online: https://www.batteryspace.com/prod-specs/5101_2.pdf (accessed on 2 March 2021).
28. Gregory L. Plett, Extended Kalman filtering for battery management systems of LiPB-based HEV battery packs: Part 1. Background. *J. Power Sources* **2004**, *134*, 252–261.